

This report has been reproduced directly from the best available copy.

Available to DOE and DOE contractors from the Office Of Scientific and Technical Information, P.O. Box 62, Oak Ridge, TN 37831; prices available from (615)576-8401, FTS 626-8401.

Available to the public from the National Technical Information Service, U.S. Department of Commerce, 5285 Port Royal Rd., Springfield, VA 22161

Price: Printed A03
Microfiche A01

**STEADY-STATE, VAPOR-LIQUID CONCURRENT FLOW:
RELATIVE PERMEABILITIES AND END EFFECTS**

Topical Report

By
Mehmet Parlak
Murat Zeybek
Yanis C. Yortsos

June 1990

Work Performed Under Contract No. FG19-87BC14126

Prepared for
U.S. Department of Energy
Assistant Secretary for Fossil Energy

Thomas B. Reid, Project Manager
Bartlesville Project Office
P.O. Box 1398
Bartlesville, OK 74005

Prepared by
University of Southern California
Department of Petroleum Engineering
Los Angeles, CA 90089-1211

Contents

List of Figures	ii
List of Tables	iii
ABSTRACT	1
INTRODUCTION	2
FORMULATION	4
CAPILLARY HETEROGENEITY	7
SATURATION-TEMPERATURE TRAJECTORIES	9
PARAMETER SENSITIVITY	13
CONCLUDING REMARKS	16
REFERENCES	18
APPENDIX	20

List of Figures

1	Capillary Heterogeneity: Saturation and Temperature Response for a Step Increase in Permeability.	25
2	Capillary Heterogeneity: Saturation and Temperature Response for a Step Decrease in Permeability.	26
3	Effect of Energy Injection Rate C (btu/hr) on Saturation and Temperature Profiles.	27
4	Capillary Heterogeneity: Effect of Conductivity for a Step Increase in Permeability (λ in $W/m^{\circ}K$).	28
5	Capillary Heterogeneity: Saturation and Temperature Response for an fbm Permeability Profile ($H = 0.7$).	29
6	Phase Portrait and (T, S) Trajectories Schematic. Arrow Indicates Upstream Direction.	30
7	Phase Portrait and (T, S) Trajectories for Water at Conditions of Table 2. Arrow Indicates Upstream Direction.	31
8	Phase Portrait and (T, S) Trajectories for Propane at Conditions of Miller (1951). Arrow Indicates Upstream Direction.	32
9	Phase Portrait and (T, S) Trajectories for Water at Conditions of Table 2. Effect of Permeability. Arrow Indicates Upstream Direction.	33
10	Sensitivity of Saturation Profiles to the Rate Parameter R_m ($R_m = 0.01, 1, 10$ from top to bottom).	34
11	Sensitivity of Inlet Saturation (S_0) to the Rate Parameter R_m for Standard Conditions: Effect of Heat Injection Rate C (btu/hr).	35
12	Sensitivity of Inlet Saturation to Steam Quality and Heat Injection Rate for the Conditions of Sanchez and Schechter (1987).	36
13	Sensitivity of Error Estimate to the Rate Parameter R_m for Standard Conditions: Effect of Heat Injection Rate C (btu/hr).	37
14	Sensitivity of Inlet Saturation and Error Estimate to the Rate Parameter R_m for Standard Conditions and Permeability of $0.005d$	38
15	Sensitivity of Inlet Saturation and Error Estimate (at two different magnifications) to the Rate Parameter R_m for Conditions of Run 15 in Sanchez and Schechter (1987).	39

List of Tables

1	List of Dimensionless Parameters and Variables	22
2	Typical Values of Variables and Parameters for Water Vapor-Liquid Flow	23
3	Typical Values of Variables and Parameters for Propane Vapor-Liquid Flow	24

STEADY-STATE, VAPOR-LIQUID CONCURRENT FLOW: RELATIVE PERMEABILITIES AND END EFFECTS

M. Parlar, M. Zeybek and Y.C. Yortsos

ABSTRACT

Steady-state methods are commonly used for the determination of the relative permeabilities of single component vapor-liquid systems, such as steam-water. Even though such experiments are performed under adiabatic conditions, the interpretation of results has proved to be a difficult task in many cases. Reasons involve phase change, heat transfer, capillarity and rate considerations.

This paper presents a systematic study of the saturation and temperature distributions in steady-state, vapor-liquid flows and examines the sensitivity to parameters such as injection rate, permeability and core length. Two sets are analyzed, one pertaining to the simultaneous injection of a two-phase mixture (Sanchez and Schechter, 1987) and another involving phase change (liquid to vapor) within the core (Miller, 1951). End effects and, in general, effects associated with capillary heterogeneity are analyzed in detail.

First, we extend our recent results for immiscible, two-phase flow (Yortsos and Chang, 1990) to account for phase change and heat transfer. It is shown that in regions of permeability decrease (increase), consecutive condensation and evaporation (evaporation and condensation) take place. Temperature gradients develop in regions of permeability increase, while almost flat profiles accompany the permeability decrease. These trends are consistent with experimental observations. The effect of thermal conductivity can be significant.

Subsequently, solution trajectories in the temperature-saturation plane are constructed. They allow a unified approach to the two problems (two-phase or single-phase injection), which are shown to lie on different parts of the same trajectory. The phase portrait obtained is found to be sensitive to variations in permeability and thermal conductivity. Minimum conditions for the development of in-situ evaporation are also developed.

Finally, the process sensitivity to parameter values is examined for two-phase injection, a typical process in relative permeability estimation. For fixed outlet-end conditions and enthalpy of injected fluids, the inlet saturation is determined as a function of a macroscopic capillary number. It is found that a plateau region develops, within which the inlet saturation is approximately constant, although corresponding saturation profiles are not necessarily flat. Numerical estimates show that

the error involved increases with decreasing enthalpy and decreasing permeability.

INTRODUCTION

The concurrent flow of a liquid and its vapor in a porous medium has been the subject of several experimental studies in the past. With main objective the estimation of vapor-liquid relative permeability pairs, simultaneous flows at steady-state and under adiabatic conditions have been investigated. Two flow configurations are typical: one involving the simultaneous injection of both vapor and liquid (e.g. steam-water), and another involving the injection of subcooled liquid only, that subsequently undergoes a phase change somewhere within the porous medium. Recent references for the former include Trimble and Menzie (1975), Monsalve et al. (1984), Verma (1986), Verma and Pruess (1986), and Sanchez and Schechter (1987). The in-situ evaporation of a flowing liquid has been examined in an early paper by Miller (1951) using propane, and in a more recent application by Counsil (1979) using water. In-situ phase change of a similar type, but with mass transfer the predominant transport process, has also been described (Handy, 1957).

While their relevance in modeling the condensing or evaporating flows, typical of thermal and geothermal processes, has not been rigorously established, and may in fact be questionable, steady-state relative permeability experiments are nonetheless attractive, due to their relative simplicity and for their own sake. Phase change introduces additional novel elements, absent from two-phase, two-component flows ("oil-water"), such as volumetric changes and heat transfer. Thus, despite the adiabatic conditions, fluid flow, phase change and heat transfer are nonetheless coupled to each other in all such experiments.

Analyses of the saturation, temperature and pressure profiles are usually obtained by decoupling fluid flow from heat transfer. An exception is the study by Verma (1986), who presented sample numerical results with the use of a general geothermal simulator previously developed (Pruess, 1982). Capillary pressure is also typically omitted, although Sanchez and Schechter (1987) make use of a Leverett J function to relate vapor and liquid pressures. The latter authors implicitly assume that flat saturation profiles are established throughout the core. Although it is likely that approximations and assumptions made in previous studies were indeed justifiable, quantitative assessments have not been provided. Equally lacking are sensitivity analyses of the effects of the various parameters.

The need for a more detailed description is underscored by the wide variation and scatter in

relative permeability curves obtained by different investigators for relatively similar porous media. Instructive is the steam-water system, of interest both to thermal recovery of oil and to geothermal energy. Trimble and Menzie (1975) report unusually low vapor (and high liquid) permeabilities, in all but a narrow region of low water saturation. In contrast, Council's (1979) data indicate an opposite effect, the vapor permeability being large (and the liquid permeability being small) in all but a narrow region of high water saturation. Trends somewhat similar to the latter were reported by Monsalve et al. (1984), the vapor permeability exhibiting a sharp decrease above a certain water saturation. On the other hand, recently obtained data contradict most of the previous, in that the relative permeabilities reported are more representative of a gas-liquid system (Verma and Pruess, 1986, and Sanchez and Schechter, 1987). Significant differences between the two pairs are claimed by the first authors, while a strong case is made by the latter authors for the similarity in relative permeabilities of vapor-liquid and gas-liquid pairs.

Theoretical work to model such flows at the micro-level has been limited. Besides the popular to the geothermal literature, but otherwise unsupported, model of straight-line relative permeabilities, the only work to address such issues was undertaken by Parlari and Yortsos (1987), and by Yortsos and Parlari (1989), in the context of steam-water, and solution gas drive, respectively. Both papers are restricted to the quasi-static limit, however, where temperature and pressure gradients are small, thus relative permeabilities are only saturation (and history) dependent. It must be noted that the model of Parlari and Yortsos (1987) for drainage does indeed corroborate the findings of Sanchez and Schechter (1987). Nevertheless, additional work is needed to support this result and to resolve other issues.

The wide experimental discrepancy calls to question the data interpretation, particularly in regions where the sensitivity to parameter values is high. Variables such as vapor (steam) quality, mass and energy injection rates, pressure, permeability and system length, all affect significantly saturation and temperature profiles. End effects are accompanied by evaporation-condensation phenomena adding yet another degree of complexity. A comprehensive analysis of such issues is not currently available. This forms the motivation for this paper. We consider the simulation of steady-state, vapor-liquid, concurrent flow, as a result of either simultaneous injection or evaporation in situ. Following a conventional approach, we formulate a complete model of the process and we proceed to examine its sensitivity to various parameters. The work presented is a sequel of a

previous study on countercurrent flows (Satik et al., 1989). As the object of this investigation is experiments in laboratory cores, end effects are addressed by generalizing recently developed methods (Yortsos and Chang, 1990) to single-component phases.

The paper is organized as follows: The formulation of the problem for adiabatic injection in 1-D geometries is, first, presented. The approach is conventional, in that relative permeabilities that depend only on saturation are considered. Clearly, this constraints what follows to relatively small saturation and temperature gradients. For completeness, Kelvin effects are also included, although they are practically insignificant everywhere, but in the very low water saturation region (see also Satik et al., 1989). We subsequently examine saturation and temperature profiles across regions of permeability (capillary) heterogeneity, in order to generalize end effects (in the manner of Yortsos and Chang, 1990). Extrapolation of the results to infinitely sharp permeability contrast yields conventional end effects. The subsequent section deals with the construction of saturation-temperature paths (trajectories) from the solution of the flow problem. Simultaneous injection or injection of a single (subcooled) liquid phase are represented by different regions of the same trajectory. Finally, saturation and temperature profiles are discussed and sensitivity studies are performed in the final section.

FORMULATION

We consider the concurrent 1-D, horizontal flow of a single-component liquid and its vapor, under steady-state, adiabatic conditions. For purposes of generalizing end effects, a heterogeneous core is assumed. We proceed with mass balances for both vapor and liquid

$$\frac{\partial}{\partial x}(\rho_v q_v) + \dot{m} = 0 \quad (1)$$

$$\frac{\partial}{\partial x}(\rho_L q_L) - \dot{m} = 0 \quad (2)$$

where \dot{m} is the condensation rate. The overall mass balance reads

$$\frac{\partial}{\partial x}(\rho_L q_L + \rho_v q_v) = 0 \quad (3)$$

and upon integration

$$\rho_L q_L + \rho_v q_v = m_L + m_v = m_i \quad (4)$$

where m_i is the mass injection rate. The conventional expressions for Darcy's law are next taken

$$q_v = -\frac{k(x)}{\mu_v} k_{rv}(S) \frac{dP_v}{dx} \quad (5)$$

$$q_L = -\frac{k(x)}{\mu_L} k_{rL}(S) \left[\frac{dP_v}{dx} - \frac{dP_c}{dx} \right] \quad (6)$$

A capillary pressure curve in terms of a Leverett J function is assumed

$$P_c = \frac{\sigma}{\sqrt{k}} J(S) \quad (7)$$

while the vapor pressure is approximated by a Clausius-Clapeyron-Kelvin expression

$$P_v = P_{v0}(T_r) \exp \left[\frac{L_{vr}}{\bar{R}} \left(\frac{1}{T_r} - \frac{1}{T} \right) - \frac{v_L}{RT} P_c \right] \quad (8)$$

More accurate phase equilibria can be used, although expected gains are not significant. For numerical purposes, relative permeability and capillary pressure curves are approximated by the simple, ad hoc expressions of Table 1. For generality, Kelvin effects were also included above, although their contribution is quantitatively negligible (except in the region of low liquid saturation).

The energy balance completes the formulation

$$\frac{\partial}{\partial x} \{ \rho_L q_L h_L + \rho_v q_v h_v \} = \frac{\partial}{\partial x} \left(\lambda \frac{\partial T}{\partial x} \right) \quad (9)$$

to yield upon subsequent integration

$$\rho_L q_L h_L + \rho_v q_v h_v = \lambda \frac{dT}{dx} + C \quad (10)$$

The constant of integration, C , is the enthalpy injection rate, and can be related to either injection or production values. For example, using injection data (subscript 0), we obtain

$$C = m_i * \{ (h_{Lr} + \chi_0 L_{vr}) + [c_{pL} - \chi_0 * (c_{pL} - c_{pv})] * (T_0 - T_r) \} - \lambda \left. \frac{dT}{dx} \right|_0 \quad (11)$$

with χ_0 denoting vapor quality at injection and where subscript r indicates reference temperature.

After lengthy manipulations the above formulation is further recast in terms of two coupled differential equations, one for the saturation and another for the temperature distributions. In the general case of variable permeability, the system has the form

$$\frac{dJ}{dS} \frac{dS}{d\xi} = R_m \frac{F(\Theta, S; \xi)}{H(\Theta, S; \xi)} \quad (12)$$

$$\frac{d\Theta}{d\xi} = R_m \frac{G(\Theta, S)}{H(\Theta, S; \xi)} \quad (13)$$

where specific expressions for $F(\Theta, S; \xi)$, $G(\Theta, S)$ and $H(\Theta, S; \xi)$ are given in the Appendix. The notation is dimensionless, with the reference temperature T_r and the core length L normalizing temperature and distance, respectively.

The system (12)-(13) contains all significant effects, including capillarity, heat conduction and phase change, summarized for convenience in Table 1 in terms of dimensionless parameters. Numerical estimates for typical conditions corresponding to the data of Sanchez and Schechter (1987) and Miller (1951) are given in Tables 2 and 3, for water and propane, respectively. Among the important variables are the macroscopic capillary number R_m , which scales rate, the parameter C/m_i , expressing enthalpy input per flowing mass, and the parameter R_h , representing the relative importance of heat conduction. In the absence of the latter or for high permeability media ($R_h \ll 1$), saturation and temperature equations decouple from each other, an assumption often used.

The solution of (12)-(13) is not as straightforward as it might appear. Solving the problem given inlet saturation and temperature values is highly sensitive to the initial conditions, particularly near inlet saturations for which flat profiles are expected. This sensitivity is not specific to this problem, but also exists for non-condensing flows as well (Yortsos and Chang, 1990). A backwards integration is thus necessary, requiring in turn that conditions at the outlet end be specified. This necessitates that end effects be addressed.

Conventional end effects correspond to large changes (orders of magnitude) in permeability over a small space interval. This can be considered as a special limit of the more general case of capillary heterogeneity across an arbitrary permeability profile. The results obtained from such study may then be applied to the special case corresponding to inlet or outlet end effects. This approach is taken in the next section.

CAPILLARY HETEROGENEITY

The saturation profiles for the 1-D flow of two immiscible, non-condensing phases in heterogeneous cores were studied in two recent publications (Yortsos and Chang, 1989, 1990). The results showed that, as a rule, the wetting phase saturation responds to a capillary (permeability) heterogeneity by exhibiting a Λ -like kink, in the case of a step-like permeability increase, and a V-like kink in the opposite case. In principle, similar effects would be anticipated for the present case. However, the coupling with the energy balance, and the temperature response itself, need further study.

Using backwards integration, the set (12)-(13) was numerically simulated for the standard conditions of Table 2 and for a step-like increase in permeability (Figure 1). The saturation response has features similar to those for flow of non-condensing phases (Yortsos and Chang, 1990): There is a build-up of the wetting (liquid) saturation in the region preceding the heterogeneity, and a subsequent decline to the original level, the latter variation confined entirely within the region of permeability change. Furthermore, for the present case, the saturation change is accompanied first by condensation and increased temperature gradients, and subsequently by evaporation and a gradual decrease of the temperature gradient.

Analogous behavior is shown in the case of permeability decrease (Figure 2). Now, the liquid saturation decreases in the region preceding the heterogeneity, giving rise to evaporation and lower temperature gradients. As in the previous, the original saturation value is rapidly restored by subsequent increases in saturation and temperature gradients, all taking place inside the heterogeneity interval.

It was previously stated that this response exhibits all the characteristics of the two-component, two-phase problem (Yortsos and Chang, 1990). This should be the case in the limit of negligible conduction ($R_h \ll 1$), negligible Kelvin effects, and constant latent heat L_v , where the two problems become mathematically identical. Indeed, at such conditions, the problem (12)-(13) decouples and takes the form

$$\epsilon \frac{dJ}{dS} \frac{dS}{d\xi} = \left\{ \frac{E}{WR_m} - F_L + \frac{\epsilon F_L k_{rv} J}{2\sqrt{k_D}} \frac{dk_D}{d\xi} \right\} \div k_{rv} F_L \sqrt{k_D} \quad (14)$$

$$\epsilon \frac{dA}{d\xi} = - \frac{(1 - (E/W R_m))}{k_{rv} k_D} \quad (15)$$

where parameter $\epsilon = R_\mu R_\rho / R_m$ as the relevant macroscopic capillary number. In the above the fractional flow F_L expresses a flowing liquid mass fraction,

$$F_L \equiv \frac{1}{1 + (k_{rv}/k_{rL}) R_\mu R_\rho} \quad (16)$$

the viscosity ratio being replaced by the ratio of kinematic viscosities $R_\mu R_\rho$. By expressing the injected fraction in terms of the injected vapor quality, χ_0

$$\frac{E}{W R_m} = \frac{m_i h_v - C}{m_i L_v} \simeq 1 - \chi_0 \quad (17)$$

the saturation equation (14) is identical to that for non-condensing flow (Yortsos and Chang, 1990). The energy balance (15) expressed in terms of the normalized vapor pressure, A , can subsequently be solved. At such conditions, all the saturation features follow readily by the analysis in Yortsos and Chang (1990).

Extrapolation of the results to conventional outlet end effects is straightforward. Assuming that a single-phase region does not develop prior to exit, the “infinitely” sharp increase in permeability induces a maximum liquid saturation buildup, therefore a complete condensation at the outflow end, which is accompanied by sharp temperature gradients and a relatively significant temperature decrease. Phase equilibria regarding exit pressure and temperature are implied in the above. When this is not the case (single phase flow conditions with either superheated vapor or subcooled liquid), end effects are absent. Extrapolation to inlet end effects is also straightforward, although not strictly applicable. Nonetheless, one tentatively expects evaporation and flat temperature profiles prior to inlet. Outlet end effects for typical conditions in homogeneous cores are illustrated in Figure 3.

Subsequently, the effect of thermal conductivity was considered. From the definition of R_h , thermal conductivity can be significant at low enough permeabilities. Figure 4. shows the response obtained for a several-fold increase in conductivity, other parameters being identical to those in Figure 1. , with the exception of the permeability variation. We observe that while temperature profiles become smoother, as expected, the saturation response is significantly affected, the capillary heterogeneity being felt over a region substantially larger than in the small conduction case.

Likewise, outflow end effects become substantial. The conduction term not being negligible, the postulated analogy in (14)-(17) with the results of Yortsos and Chang (1990) is no longer valid, and further study is needed. We must stress that although the profiles in Figure 4. are for high conductivities, similar effects are also expected for typical values in low permeability cores, in view of the scaling properties of R_h .

For completeness, we also present saturation and temperature profiles corresponding to a heterogeneity (permeability) field that obeys fractal statistics (fractional Brownian motion, fBm). The relevance of fBm statistics to field heterogeneity was conjectured by Hewett (1986). Results for $H = 0.7$, corresponding to a fractal dimension $D = 1.3$ (Feder, 1988), are shown in Figure 5. The permeability field having long-range correlations ($H > 0.5$), permeability gradients are generally small, thus the saturation response is relatively mild (although sharp responses are expected for negatively correlated fields, $H < 0.5$, see Yortsos and Chang, 1990). Even smaller is the effect on the temperature profile.

In the above, rate conditions were selected such that flat saturation profiles were likely to develop over most of the core extent (see also related discussion below). Contrary to non-condensing flows, however, flat saturation profiles in vapor-liquid flows cannot be extended indefinitely. Beyond a certain interval, liquid saturations start to slowly increase in the upstream direction, and conditions of single-phase liquid flow eventually set. From the conventional forward direction, these processes correspond to the in-situ change of phase described by Miller (1951), Handy (1957) and Council (1979). To obtain useful information about such flows the corresponding saturation-temperature trajectories must be examined.

SATURATION-TEMPERATURE TRAJECTORIES

For the remainder, homogeneous cores only will be considered. Here, saturation and temperature are uniquely related, as can be seen by eliminating from (12)-(13) the space variable. The solutions of the resulting equation constitute trajectories in the "phase (composition) space," each corresponding to a specific initial (outlet end) condition. The display (phase portrait) of such trajectories is of interest, as it allows for qualitative conclusions to be reached. Since our main interest is in two-phase flow, initial conditions at the outflow end will be specified, by taking variable temperatures and either $S = 1$ or $S = 0$. This particular selection of saturation values is necessitated by end effects (saturation, slightly subcooled or slightly superheated conditions, respectively). The

precise specification requires precise knowledge of the exit conditions, a rather difficult task in practical applications. We shall return to this issue below.

For convenience, we rewrite the trajectory equation to be solved in the form

$$\frac{dJ}{dS} \frac{dS}{d\Theta} = \frac{F(\Theta, S)}{G(\Theta, S)} \quad (18)$$

where, in the absence of heterogeneity

$$F(\Theta, S) \equiv \frac{KR_p A}{\Theta^2} \left(W - \frac{E}{R_m} \right) k_{rL} + \frac{KR_p A}{\Theta^2} \left(-\frac{E}{R_m} \right) R_\mu R_p k_{rv} + R_h \quad (19)$$

$$G(\Theta, S) \equiv (1 + bR_p A) \left(W - \frac{E}{R_m} \right) k_{rL} + bR_p A \left(-\frac{E}{R_m} \right) R_\mu R_p k_{rv} \quad (20)$$

For negligible Kelvin effects we may further approximate

$$G(\Theta, S) \simeq \left(W - \frac{E}{R_m} \right) k_{rL} \quad (21)$$

Expressions for the heat input rates $W - (E/R_m)$ or $-E/R_m$ are given in the Appendix.

An important element of the phase portrait is the critical curve $F(\Theta, S) = 0$ (curve *A* in Figure 6.), which controls the sign of the saturation slope dS/dx . Of less importance is the other critical curve $G(\Theta, S) = 0$ (curve *B* in Figure 6), which controls the sign of the temperature slope dT/dx . The two curves divide the (Θ, S) plane into three regions: Trajectories in regions I and III have negative slope that depends mainly on R_h , while those in II have positive slope. The dividing curves *A* and *B* approach each other near $S = 1$, at which point (*D* in Figure 6), for $R_h \ll 1$, the corresponding temperature, T_2 , is the solution of

$$h_L(T_2) = \frac{C}{m_i} \quad (22)$$

This is the temperature at which the saturated liquid has the enthalpy of the injected fluid. We note that for other parameters kept fixed, the phase portrait is a function of the injected energy per unit mass, C/m_i . An increase in the latter leads to an enlargement of region I, towards higher temperatures and lower saturations.

It is of interest to follow a typical trajectory. We consider, first, trajectories starting from the axis $S = 1$ (point O). While in region I, the trajectory has a (slightly) negative slope, reflecting the small temperature increase as the saturation decreases in the upstream direction (indicated by the arrow). This slope can be substantial when parameter R_h is large (e.g. small k or large λ). It is in this region that capillary end effects are significant, and in fact, region I is essentially a magnification of the boundary region near the outlet end (Figure 3). One should note that the saturation spatial profile does not become flat until the critical curve A is encountered.

Upon approach of curve A , the function F , thus the saturation slope, become very small, and the corresponding saturation profile is nearly flat. This is also reflected in the direct integration of the previous set (12)-(13) in this region which is extremely slow, and has, in fact, prompted us into using (18) as an alternative to direct integration. Subsequently, the trajectory crosses over A at the turning point (C in Figure 6), where F changes sign, region II is entered, and the trajectory changes direction and acquires a positive slope. Curve A acts now as an attractor, the solution trajectory becoming almost indistinguishable from it to the printer's resolution. Both saturation and temperature increase in the direction of the arrow (upstream), until single-phase flow conditions are approached (point D). In this region, all trajectories, regardless of their initial (outlet) condition practically coincide with curve A , implying that all in-situ vaporization regimes lie on the same curve for constant enthalpy content C/m_i .

Similar results are obtained for solution trajectories that emanate from the axis $S = 0$, instead (point O' in Figure 6). Such trajectories have a slightly negative slope in region III, while being practically flat in most of region II. As in the previous, however, flat saturation spatial profiles are encountered only when the critical curve A is approached (C'). Thereafter, the trajectory becomes attracted to A , which it closely follows until the single-phase point D . In fact, the two different trajectories (whether starting from the "liquid" or the "vapor" side) coincide for all practical purposes away from the boundaries. We should mention that similar effects were also observed in the related study of countercurrent vapor-liquid flow (Satik et al., 1989).

Before proceeding further, several remarks are appropriate. We, first, note that such phase portraits unify the different two-phase flow regimes that develop in the two kinds of experiments, e.g. the Sanchez and Schechter (1987) or the Miller (1951) type. The former case (most appropriate for relative permeability measurements) corresponds to the segments CO (or $C'O'$) where capillary end

effects can be important. Clearly, starting (injection) points can be anywhere along the trajectory, and they are determined by the rate parameter, R_m (see also below). In the absence of additional information the precise path selection (CO vs. $C'O'$) may be unclear. However, the (slightly) negative slope in region III implies a temperature increase in the downstream direction near the outlet end, for trajectories emanating from $S = 0$. This leads us to tentatively conjecture against the existence of such solutions at steady-state. However, additional work is needed to conclusively resolve this issue.

The other case involves the entire trajectory (DCO) and corresponds to evaporation in situ. Again, the selection of the particular route (DCO or $DC'O'$) for fixed outflow end temperature is uncertain. However, the practical consequences of this uncertainty are not significant in the present case, since the relative length of the last segment (CO or $C'O'$ vs. DCO or $DC'O'$) is negligible. Because of this, experiments of this type are likely to offer useful information only as it regards saturations in the main path DC (or DC').

The physical meaning of curve A is the condition of constant enthalpy flow in the absence of capillarity (relatively high values in R_p). This is most readily seen in the no-conduction limit, where in dimensional notation one obtains

$$\frac{k_{rL}}{R_\mu R_\rho k_{rv}} = -\frac{h_v(T) - (C/m_i)}{h_L(T) - (C/m_i)} \quad (23)$$

By rearrangement, it is easily shown that (23) indeed expresses the adiabatic condition of constant enthalpy in the absence of capillary and heat conduction effects. We note that at such conditions, this is essentially the solution of Miller in his original paper (1951). In fact, the entire curve A can be readily transformed into the "pressure function" considered by Miller (1951) by a simple change of variables. By further neglecting the variation of latent heat with temperature, the critical curve becomes vertical (constant S)

$$F_W(S) = 1 - \chi_0 \quad (24)$$

and where χ_0 is the injected vapor quality (compare with previous section). Temperature and heat conduction effects cause the notable departure from the vertical.

Trajectories for water and propane for the conditions of Tables 2 and 3 are shown in Figures 7 and 8, respectively. The attraction of the trajectories to the single critical curve is evident in both

figures. This feature is a consequence of negligible capillarity compared to the saturation pressure, particularly at higher temperatures. Parameter R_p measures this effect at reference conditions. For the case of propane at conditions of Table 3, the large value of R_p and the high permeability (low R_h) verify the correctness of the approach used by Miller (1951).

This need not be the case, however, for lower permeability (or higher conductivity) cores. The phase portrait in Figure 9 corresponds to a 100-fold reduction in permeability and shows several significant differences: The size of region I has been reduced, the critical curve A no longer coincides with the limiting curve in the absence of conduction (e.g. Figure 6), while the trajectories in region I take a significant slope, indicating the added importance of capillarity at lower permeabilities. Nevertheless, at sufficiently large temperature (pressure) all trajectories get eventually attracted to the single curve A (compare Figures 7 and 9). Additional permeability effects are presented below.

PARAMETER SENSITIVITY

The preceding section showed that for a fixed enthalpy per unit mass the phase portrait is fixed. The particular solution trajectory was then determined by the exit temperature (pressure). The spatial saturation and temperature profiles, however, depend additionally on the rate parameter R_m . This is the only length-dependent parameter. The latter determines whether evaporation in-situ (e.g. Miller, 1951) or flat saturation profiles (e.g. Sanchez and Schechter, 1987) or an intermediate regime would be established. The three possibilities are depicted in Figure 10. We point out that the saturation-temperature pairs in each of the three regimes of Figure 10, all belong to the same trajectory, each experiment representing a magnification of a region of the previous one.

Conditions for in-situ evaporation can be precisely specified. For example, the minimum length of the core required follows from the requirement that

$$R_m \geq X_2 \quad (25)$$

where X_2 depends on the energy content C/m_i and on the exit temperature (Θ_1 in dimensionless notation), and it is given from (13)

$$X_2 = - \int_{\Theta_1}^{\Theta_2} \frac{H(\Theta, S(\Theta; \Theta_1))}{G(\Theta, S(\Theta; \Theta_1))} d\Theta \quad (26)$$

The above integral is evaluated along the particular trajectory, emanating from Θ_1 , with S solving (18).

The variation of X_2 with the outlet temperature was investigated for the conditions of experiment V by Miller (1951) shown in Table 3. In general, X_2 was found to decrease as T_1 increases and as the thermal energy content C/m_i decreases. Sample values obtained were 45.7 and 19.2 for T_1 equal to 40°F and 80°F, respectively. Comparison with Table 3 shows readily that condition (25) is indeed satisfied. It was previously pointed out that experiments of this type sample regions of saturation higher than the value corresponding to the turning point, S^* . As one may expect, end effects are insignificant for in-situ evaporation. A quantitative assessment is readily obtained by comparing X_2 to X^* , where X^* is evaluated from (26) with Θ^* as the upper limit of integration. For the conditions of Table 3, one obtains $X^* = 0.15$, which is negligibly small in comparison to X_2 .

When condition (25) is not satisfied, two-phase flow occurs throughout the core. Given the exit temperature (pressure), the specific trajectory is fixed, thus saturation and temperature profiles can be determined. Inlet conditions (S_0, T_0) are obtained by solving the equation

$$R_m = - \int_{\Theta_1}^{\Theta_0} \frac{H(\Theta, S(\Theta; \Theta_1))}{G(\Theta, S(\Theta; \Theta_1))} d\Theta \quad (27)$$

and subsequently evaluating S_0 with the use of the trajectory equation (18). The integration of equation (13), rather than the saturation equation (12) must be noted. Contrary to the saturation, which exhibits a turning point, the temperature is monotonically varying, thus facilitating the integration. This aspect is particular to two-phase, single-component systems.

Typical results are shown in Figure 11, for various values of the energy content and the conditions of Table 2. As R_m increases (by increasing the total rate or the system length), S_0 decreases until the turning point value S^* is reached. A significant plateau region develops thereafter, the extent of which increases with the energy content (steam quality) and the permeability. In view of the various uncertainties involved in the estimation of parameters, the existence of such a plateau over orders of magnitude in R_m is highly desirable. Unfortunately, its size decreases significantly at lower values of C/m_i and at lower permeabilities (see below). This sensitivity is somewhat similar to that of injected quality χ_0 , exhibited in more simplistic approaches, where S^* is taken to be the solution of (24). A plot of this approximation to S^* is shown in Figure 12. The sensitivity near

low values of the injected quality is quite notable and it has been conjectured to cause errors in the estimation of relative permeabilities in that region.

The success of most relative permeability experiments relies on the condition that a flat profile be established throughout the core with S^* as the core inlet saturation. To ascertain this, the relative importance of end effects must be considered. As a measure of the deviation from flat profiles we consider the following parameter

$$\delta = \int_0^1 \left(\frac{S - S^*}{S^*} \right) d\xi \quad (28)$$

Upon rearrangement and use of (12), (13) and (18), this becomes

$$\delta = -\frac{1}{R_m} \int_{\Theta_1}^{\Theta_0} \left(\frac{S}{S^*} - 1 \right) \frac{H(\Theta, S(\Theta; \Theta_1))}{G(\Theta, S(\Theta; \Theta_1))} d\Theta \quad (29)$$

Since Θ_0 is implicitly related to R_m via (27), equation (29) gives δ as a function of R_m , other parameter kept constant.

Plotted in Figure 13 is the error estimate δ as a function of the rate parameter R_m , for the conditions of Figure 11. Roughly paralleling the inlet saturation plot (Figure 11) the error decreases considerably as R_m increases, particularly after the turning point has been exceeded. More importantly, a plateau region of small error values develop, the extent of which can be considerable for high C and k . This is highly desirable, since large variations in R_m , the proper values of which cannot be a priori known, only result in relatively small errors. Upon leaving the plateau region, however, substantial errors are rapidly established, that prohibit the successful conduct of meaningful relative permeability experiments there.

The error estimate was found to be sensitive to the injected energy content, more reliable results being obtained at higher injection quality, roughly in step with the saturation sensitivity (Figures 11 and 13). In general, the plateau extent decreases and errors increase with a decrease in the injected energy content, although the minimum error value is not as sensitive and remains low, at least for the cases studied. On the other hand, errors are uniformly higher for lower permeability cores. Plotted in Figure 14 are the inlet saturation and the corresponding error estimate for the conditions of Table 2, but with a hundred-fold reduction in permeability. It is apparent that the plateau disappears, and that only a narrow region remains, where, however, errors are significantly higher than before (the lowest value being higher than 33% in the case of Figure 14). It is clear

that meaningful relative permeability experiments of this type are not possible for such cases, and alternatives must be sought.

As a sample illustration of the above sensitivity we simulated the error involved in one of the experiments (run no.15) reported by Sanchez and Schechter (1987). Except for the capillary pressure curve (for which the expression of Table 1 was used), all other parameters including relative permeabilities were reported. The corresponding inlet saturation and error estimate plots are shown in Figure 15. Notable are the wide plateau regions and the corresponding low error values, both resulting from the large core permeability. Also marked in Figure 15 are the inlet saturation ($S_0 = 0.2927$) and error ($\delta = 7.7\%$) estimates corresponding to the experimental value for this run, $R_m = 0.015$. The relatively low error estimate, coupled with the good agreement between theoretical and experimental ($S_0 = 0.31$) values underscores the reliability of these data (although an analysis of all the runs is of course necessary for a more rigorous assessment).

CONCLUDING REMARKS

In this paper we analyzed steady-state, concurrent vapor-liquid flows in 1-D cores under adiabatic conditions. The general problem was treated including heat conduction, capillarity, phase change and Kelvin effects. The latter were found to be negligible, except at the low liquid saturation range, where, however, unaccounted thin film effects become quite important and must be included. The aim of the study was to examine the features of saturation and temperature profiles, to explore their sensitivity to process parameters, and to provide error estimates for relative permeability vapor-liquid experiments typically conducted at steady-state.

It was, first, shown that reliable numerical results are only possible by backwards (in the upstream direction) integration, a requirement that can be met only if (outlet-) end conditions are available. This led us to the analysis of end effects and, in general, of effects caused by capillary heterogeneity. For small values of the conduction parameter R_h (small conductivity or large permeability), the effects on the liquid (wetting) saturation are identical to the case of two-phase, two-component (oil-water) flow, analyzed in detail in a recent work (Yortsos and Chang, 1990). The temperature profile is also affected, becoming steeper (smoother) near the heterogeneity region for a downstream increase (decrease) in the permeability. Direct extrapolation to conventional end effects suggests a maximum liquid saturation buildup, accompanied by condensation and sharp temperature gradients at the outlet end. Opposite effects are to be expected at the inlet (although

such extrapolation may not be strictly proper). Conductivity was found to exert significant effects by extending the influence of the heterogeneity to a greater region. While unimportant for large permeability cores, such effects are quantitative for tight cores.

Subsequently, the flow in homogeneous cores was simulated in terms of temperature-saturation (composition) trajectories. This approach enables a unified approach to the vapor-liquid flow that encompasses both the in-situ vaporization of Miller (1951) (injection of a subcooled liquid) and the simultaneous injection of two-phases, as is typical in relative permeability experiments (Sanchez and Schechter, 1987). It was found that all solution trajectories are rapidly attracted (away from end effects) to the critical curve that describes flow in the absence of capillarity. It is in its near vicinity, where inlet conditions in typical relative permeability experiments also lie. Under the additional constraint of negligible conduction, this curve coincides with the solution of Miller (1951). However, significant discrepancies arise as the permeability decreases.

Based on the above, parameter sensitivity studies were conducted. Quantitative requirements on the rate parameter R_m were obtained for in-situ vaporization to occur. Typical minimum estimates range between 10 and 50 for the cases studied. The sensitivity of the inlet saturation (for fixed outlet temperature) was next considered. It was shown that a plateau-like region develops covering a range of R_m that may span several orders of magnitude, depending on the permeability primarily, and on the injected energy content, to a lesser extent. Such plateau regions are desirable, in order to suppress parameter sensitivity and related errors. An error measure was also defined and found to obey a similar dependence. The existence at high permeability values ($R_h \ll 1$) of a wide region of low errors indicates that relative permeability estimates obtained at such conditions can be reliable. A sample illustration using data from Sanchez and Schechter (1987) provides supporting evidence. On the other hand, serious questions should be raised regarding the applicability of current methods for vapor-liquid relative permeabilities of tight cores. It was shown that the lowest possible errors can be quite large, while being very sensitive to the rate parameter. We conclude that for such cases alternative methods are needed.

REFERENCES

1. Counsil, J.R., "Steam-Water Relative Permeability", Ph.D. Dissertation, Stanford University, Stanford, CA (1979).
2. Feder, J., *Fractals*, Plenum Press, New York (1988).
3. Handy, L.L., "Effect of Local High Gas Saturations", *API Drilling and Production Practices* (1957).
4. Hewett, T.A., paper SPE 15386 presented at the 61st Annual SPE Fall Meeting, New Orleans, LA (1986).
5. Miller, "Steady Flow of Two-Phase Single-Component Fluids Through Porous Media", *Trans. AIME*, **192**, 205 (1951).
6. Monsalve, A., Schechter, R.S., and Wade, W.H., paper SPE 12661 presented at the 1984 SPE/DOE Symposium on Enhanced Oil Recovery, Tulsa, OK (Apr. 1984).
7. Parlar, M., and Yortsos, Y.C., paper SPE 16969 presented at the 62nd Annual SPE Fall Meeting, Dallas, TX (Sept. 1987).
8. Pruess, K., Annual Report, Earth Sc. Div., Lawrence Berkeley Laboratory, Berkeley, CA (1982).
9. Sanchez, J.M., and Schechter, R.S., paper SPE 16967 presented at the 62nd Annual SPE Fall Meeting, Dallas, TX (Sept. 1987).
10. Satik, C., Parlar, M. and Yortsos, Y.C., "A Study of Steady- State Steam-Water Counterflow in Porous Media", submitted (1989).
11. Trimble, A.E., and Menzie, D.E., paper SPE 5571 presented at the 50th Annual SPE Fall Meeting, Dallas, TX (Sept. 1975).
12. Verma, A.K., Ph.D. Dissertation, University of California, Berkeley, CA (1986).
13. Verma, A., and Pruess, K., Proc. Eleventh Workshop on Geothermal Reservoir Engineering, Stanford U., Stanford, CA (Jan. 1986).

14. Yortsos, Y.C., and Chang, J., paper SPE 18798 presented at the 1989 California Regional Meeting, Bakersfield, CA (1989)
15. Yortsos, Y.C., and Chang, J., "Capillary Effects in Steady- State Flow in Heterogeneous Cores", *Transp. Porous Media*, in press (1990).
16. Yortsos, Y.C., and Parlar, M., paper SPE 19697 presented at the 64th Annual SPE Fall Meeting, San Antonio, TX (1989).

APPENDIX

Upon manipulation of equations (1)-(11), the following system is obtained in dimensionless notation

$$\frac{dJ}{dS} \frac{dS}{d\xi} = R_m \frac{F(\Theta, S; \xi)}{H(\Theta, S; \xi)} \quad (\text{A-1})$$

$$\frac{d\Theta}{d\xi} = R_m \frac{G(\Theta, S)}{H(\Theta, S; \xi)} \quad (\text{A-2})$$

where

$$\begin{aligned} F(\Theta, S; \xi) \equiv & \left[\frac{K R_p A}{\Theta^2} k_D^{1/2} \left(W - \frac{E}{R_m} \right) \right. \\ & + \frac{R_L (1 + b R_p A) J}{2 k_D} \frac{dk_D}{d\xi} \\ & - \left. \frac{K R_p A J W}{2 R_m \Theta^2} \frac{dk_D}{d\xi} R_\mu R_\rho k_{rv} \right] k_{rL} \\ & + \left[\frac{K R_p A}{\Theta^2} k_D^{1/2} \left(-\frac{E}{R_m} \right) \right. \\ & + \left. \frac{R_L b R_p A J}{2 k_D} \frac{dk_D}{d\xi} \right] R_\mu R_\rho k_{rv} \\ & + \frac{R_h}{k_D^{1/2}} \end{aligned} \quad (\text{A-3})$$

$$\begin{aligned} G(\Theta, S) \equiv & (1 + b R_p A) \left(W - \frac{E}{R_m} \right) k_{rL} \\ & + b R_p A \left(-\frac{E}{R_m} \right) R_\mu R_\rho k_{rv} \end{aligned} \quad (\text{A-4})$$

$$\begin{aligned} H(\Theta, S; \xi) \equiv & [R_h (1 + b R_p A) \\ & - \frac{K R_p A}{\Theta^2} k_D W R_\mu R_\rho k_{rv}] k_{rL} \\ & + R_h b R_p A R_\mu R_\rho k_{rv} \end{aligned} \quad (\text{A-5})$$

The various dimensionless terms are defined in Table 1. Important variables in what follows are R_m and R_h , the first denoting a macroscopic capillary number and the latter expressing the conduction effects. Parameter $b (\ll 1)$ is a measure of Kelvin effects, typically negligible, except at low values of the liquid saturation S . Variables $W - E/R_m$ and $-E/R_m$ represent local vapor and liquid fraction

$$W - \frac{E}{R_m} = \frac{h_L(T) - C/m_i}{L_{vr}} \quad (\text{A-6})$$

$$-\frac{E}{R_m} = \frac{h_v(T) - C/m_i}{L_{vr}} \quad (\text{A-7})$$

respectively. It must be noted that these are the only parameters that carry information about the injected enthalpy rate, C . Under isothermal conditions they simplify to

$$W - \frac{E}{R_m} = -\chi_0 \quad (\text{A-8})$$

$$-\frac{E}{R_m} = 1 - \chi_0 \quad (\text{A-9})$$

where χ_0 is the steam quality at injection. Finally, the dimensionless vapor pressure A , normalized with respect to the saturation pressure at the reference temperature is given by

$$A = \exp \left[K \left(1 - \frac{1}{T} \right) - \frac{bJ(S)}{\sqrt{k_D(\xi)}} \right] \quad (\text{A-10})$$

where use of (8) was made.

Table 1

$$\begin{array}{lll}
 R_h = \frac{\lambda T_r \mu_L}{\sigma \sqrt{k^*} \rho_L L_{\text{eff}}} & R_m = \frac{m_i \mu_L L}{\sigma \sqrt{k^*} \rho_L} & R_L = \frac{\lambda T_0 / L}{m_i L_{\text{eff}}} \\
 R_p = \frac{P_{\text{vo}}(T_r)}{\sigma / \sqrt{k^*}} & R_\mu = \frac{\mu_L}{\mu_v} & R_\rho = \frac{\rho_v}{\rho_L} \\
 K = \frac{L_{\text{eff}}}{\bar{R} * T_0} & \bar{R} = \frac{R}{M} & k_D(\xi) = \frac{k(\xi)}{k^*} \\
 \tau_{ch} = \frac{2\sigma v_L}{RT} & b = \frac{\tau_{ch}}{2\sqrt{k^*}} & \\
 \Theta = \frac{T}{T_r} & \xi = \frac{x}{L} &
 \end{array}$$

$$k_{rL} = S^{2.35}$$

$$k_{rv} = (1 - S)^{2.35}$$

$$J = 1.417(1 - S) - 2.12(1 - S)^2 - 1.263(1 - S)^3$$

Table 1: List of Dimensionless Parameters and Variables

Table 2

DIMENSIONAL VARIABLES:

Total Mass Flux, m_i (gr/hr) = 120
Exit Temperature, T_1 ($^{\circ}C$) = 100
Reference Temperature, T_r ($^{\circ}C$) = 100
Permeability, k° (darcy) = 0.5
Cross Sectional Area, (sq.cm) = 20.268
Heat Input Rate, C (btu/hr) = 100
Thermal Conductivity, λ ($\frac{W}{m^{\circ}K}$) = 2.5
Interfacial Tension, σ ($\frac{dyne}{cm}$) = 58.91
Core Length, L (cm) = 50

DIMENSIONLESS PARAMETERS :

$b = 0.000504$
 $K = 13.10923$
 $R_{\mu} = 22.41270$
 $R_{\rho} = 0.000625$
 $R_p = 1.21621$
 $R_m = 0.058034$
 $R_h = 0.002917$
 $R_L = 0.050265$

Table 2: Typical Values of Variables and Parameters for Water Vapor-Liquid Flow

Table 3

DIMENSIONAL VARIABLES:

Total Mass Flux, m_i (gr/hr) =	4699.2
Exit Temperature, T_1 ($^{\circ}C$) =	21.1 (70 $^{\circ}F$)
Reference Temperature, T_r ($^{\circ}C$) =	35.56 (96 $^{\circ}F$)
Permeability, k° (darcy) =	0.9
Cross Sectional Area, (sq.cm) =	22.018
Heat Input Rate, C (btu/hr) =	2720.3
Thermal Conductivity, λ ($\frac{W}{m^{\circ}K}$) =	2.5
Interfacial Tension, σ ($\frac{dyne}{cm}$) =	5.5
Core Length, L (cm) =	152.4

DIMENSIONLESS PARAMETERS :

b =	0.000199
K =	5.49054
R_{μ} =	12.04819
R_{ρ} =	0.056749
R_p =	213.11244
R_m =	36.4553
R_h =	0.0974
R_L =	0.0027

Table 3: Typical Values of Variables and Parameters for Propane Vapor-Liquid Flow

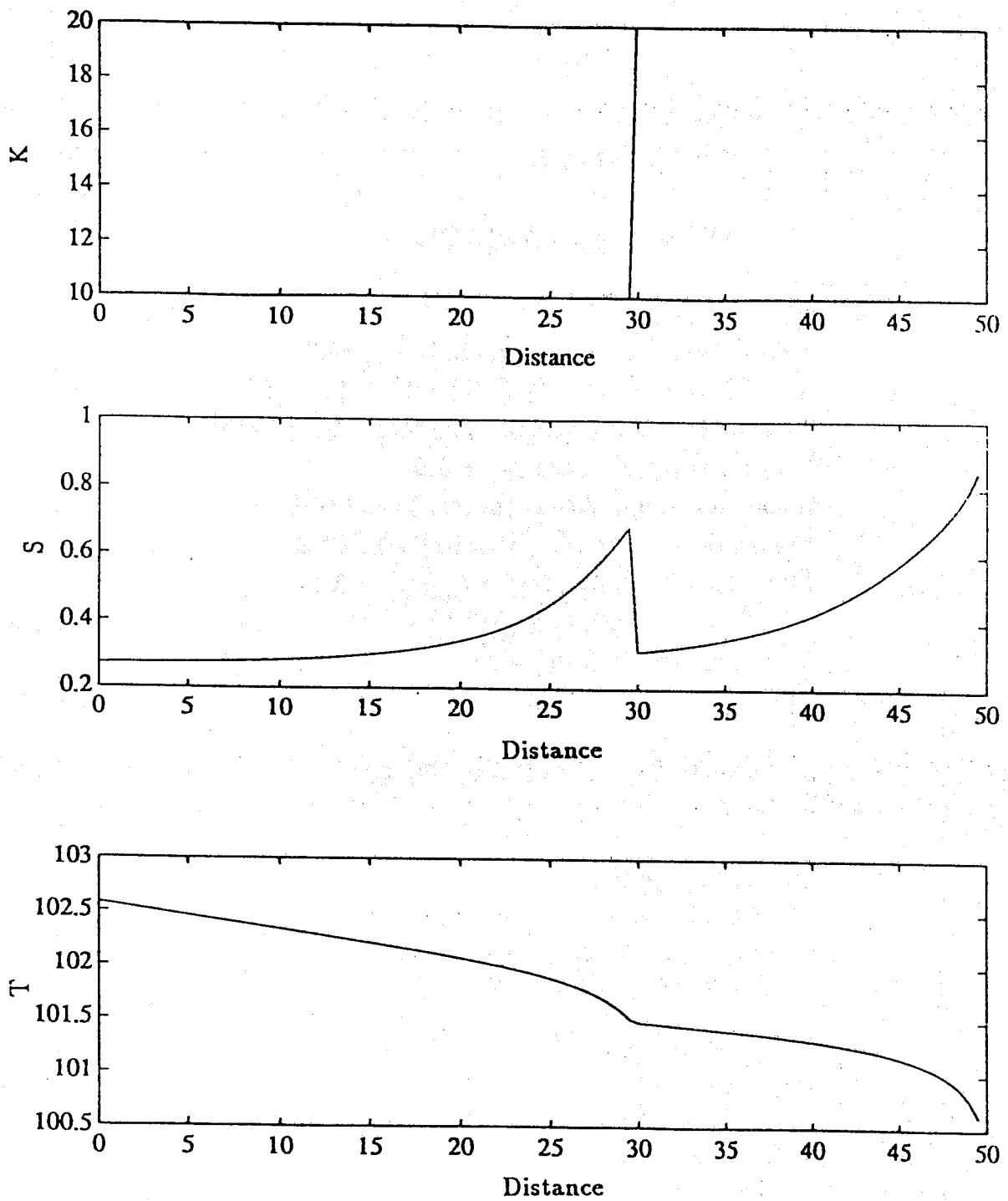


Figure 1: Capillary Heterogeneity: Saturation and Temperature Response for a Step Increase in Permeability.

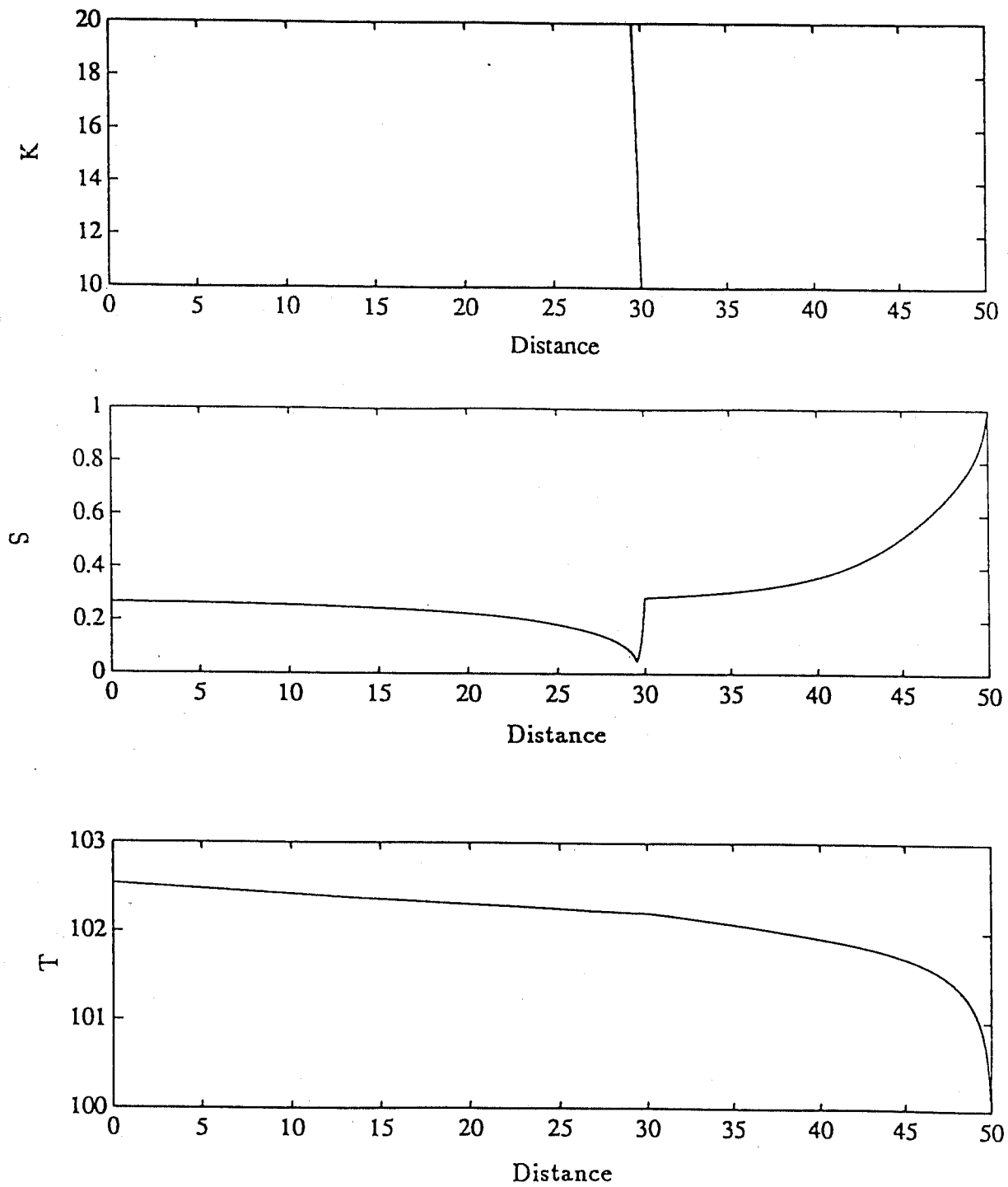


Figure 2: Capillary Heterogeneity: Saturation and Temperature Response for a Step Decrease in Permeability.

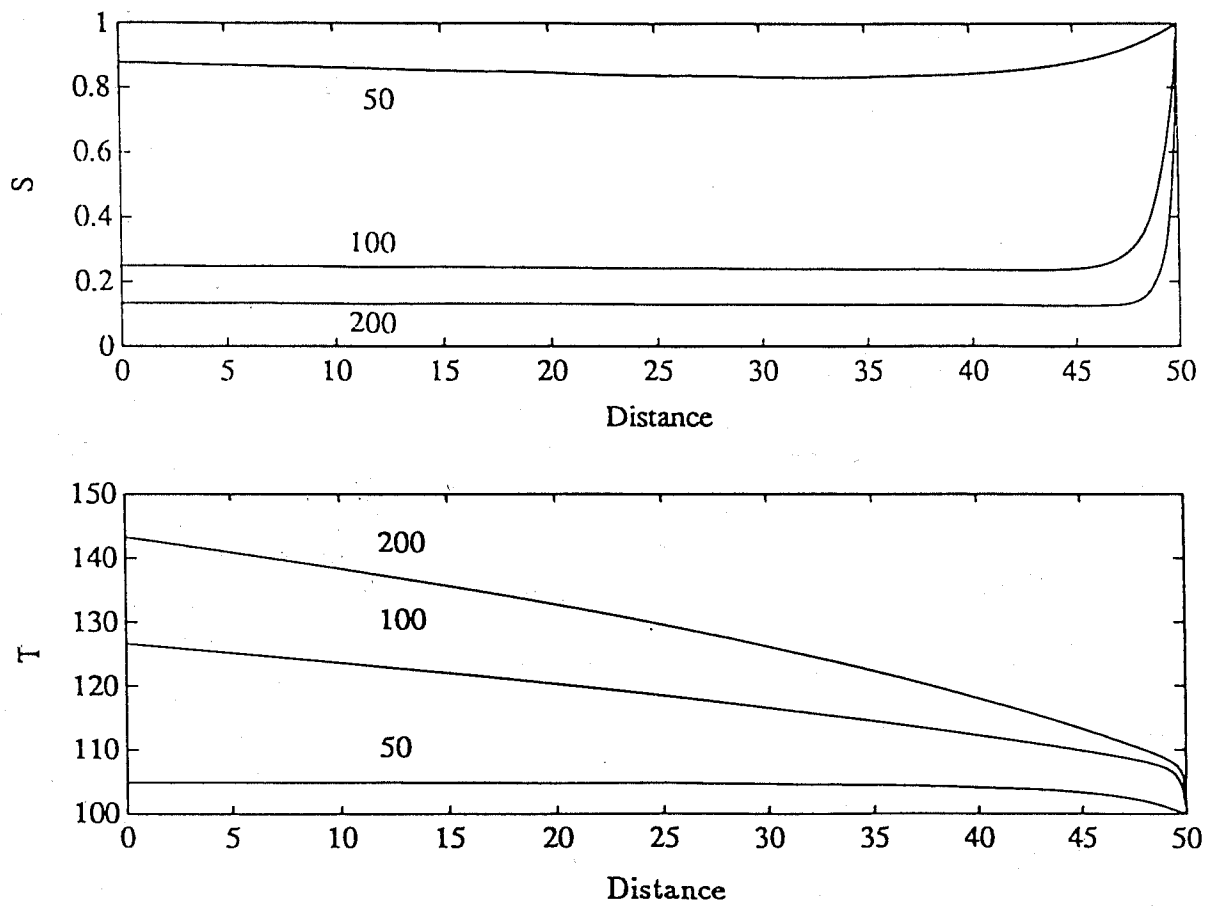


Figure 3: Effect of Energy Injection Rate C (btu/hr) on Saturation and Temperature Profiles.

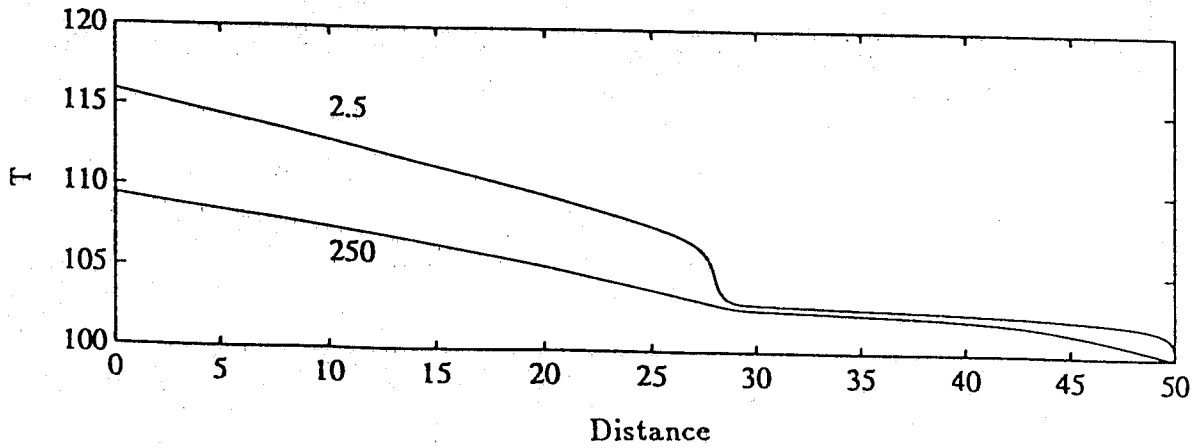
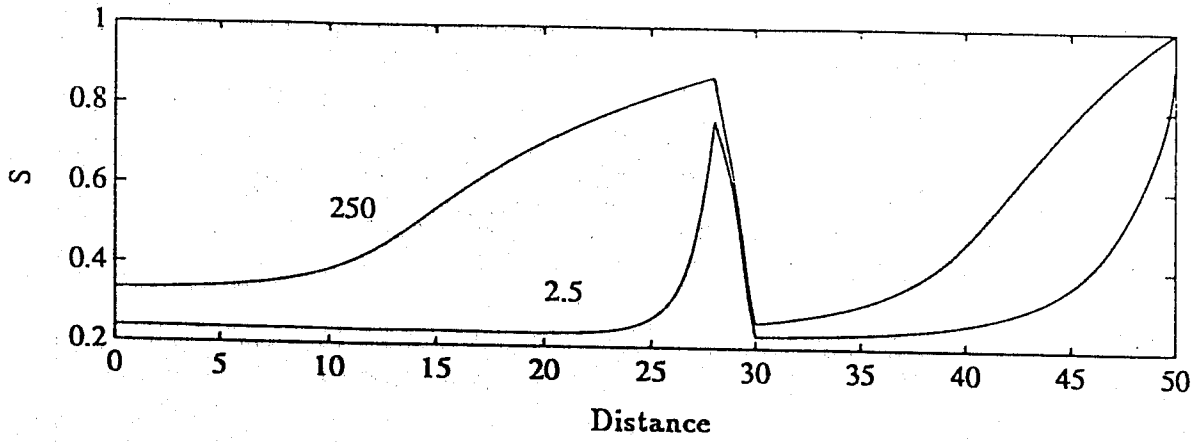
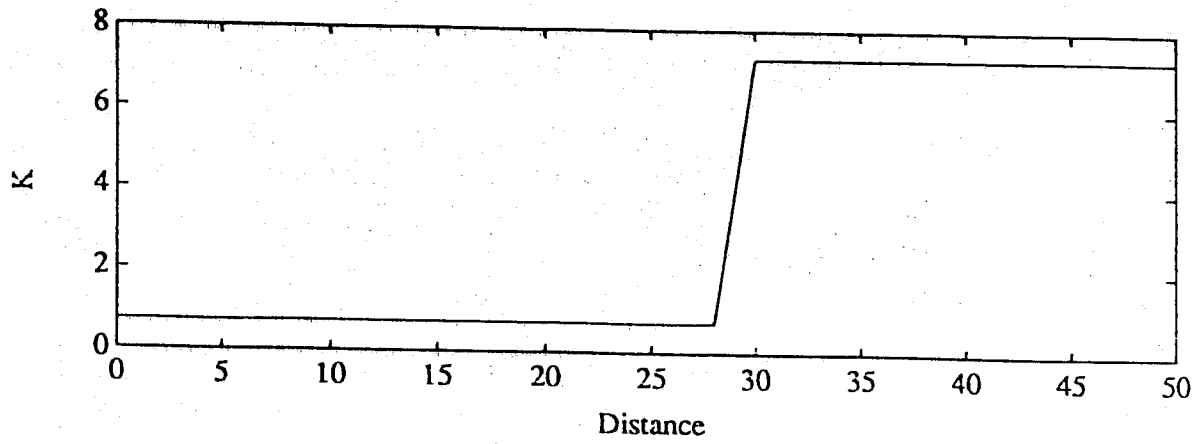


Figure 4: Capillary Heterogeneity: Effect of Conductivity for a Step Increase in Permeability (λ in $W/m^{\circ}K$).

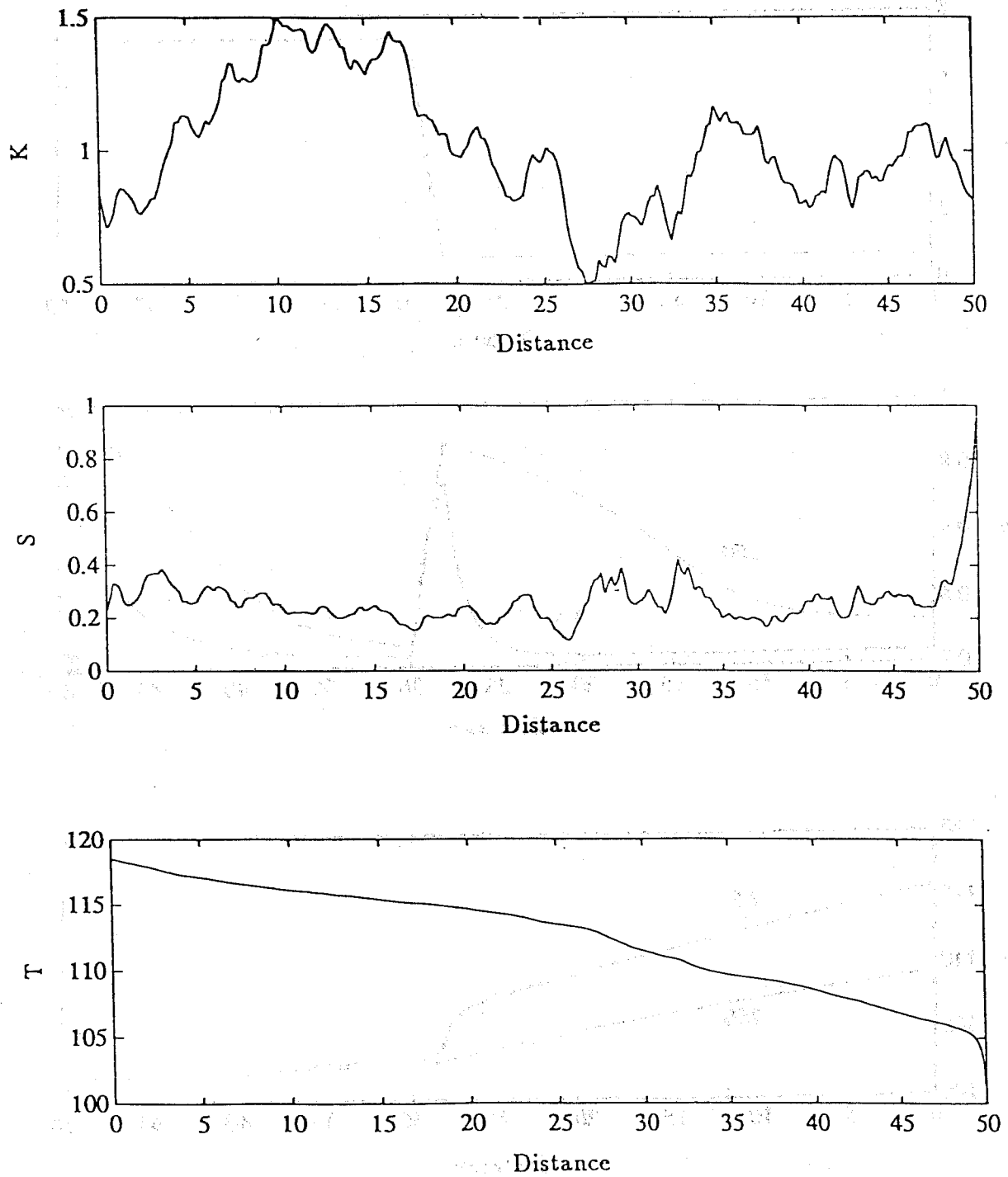


Figure 5: Capillary Heterogeneity: Saturation and Temperature Response for an fbm Permeability Profile ($H = 0.7$).

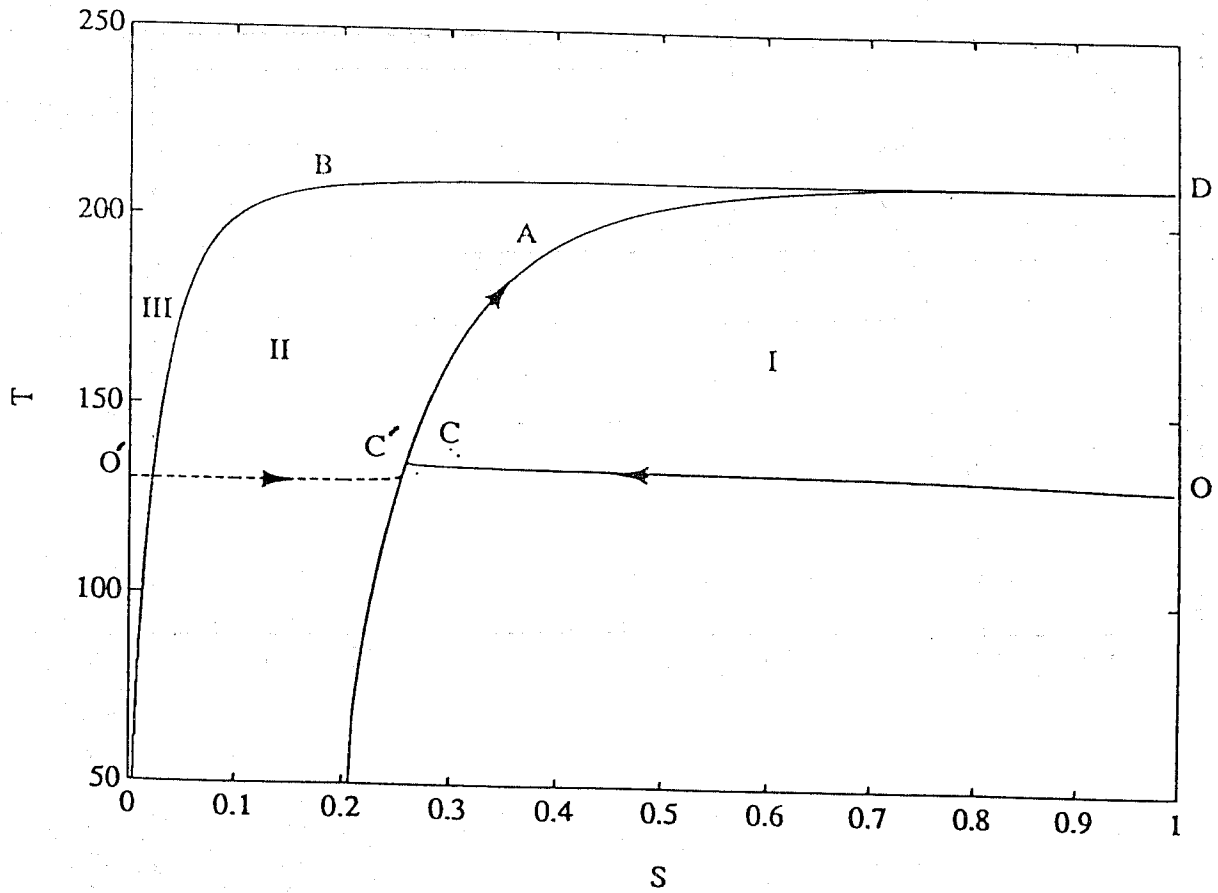


Figure 6: Phase Portrait and (T, S) Trajectories Schematic. Arrow Indicates Upstream Direction.

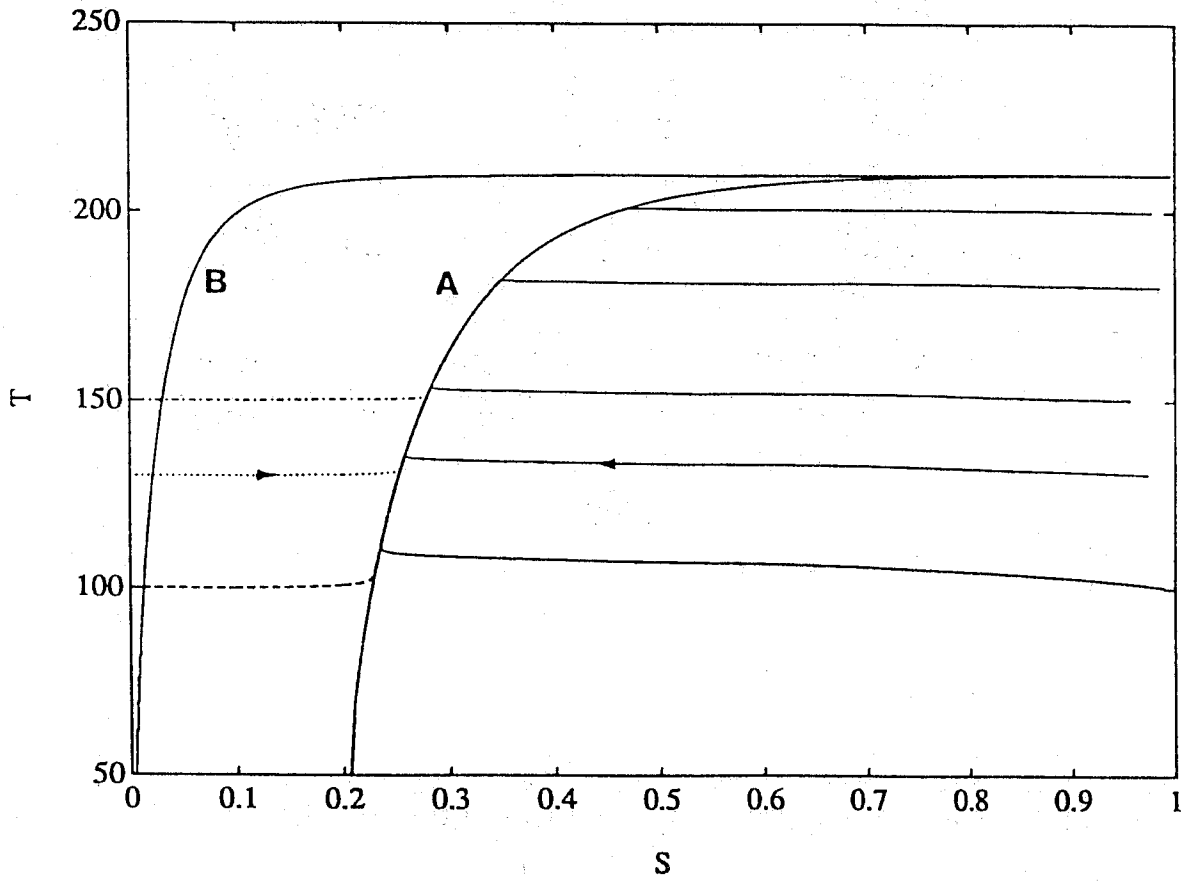


Figure 7: Phase Portrait and (T, S) Trajectories for Water at Conditions of Table 2. Arrow Indicates Upstream Direction.

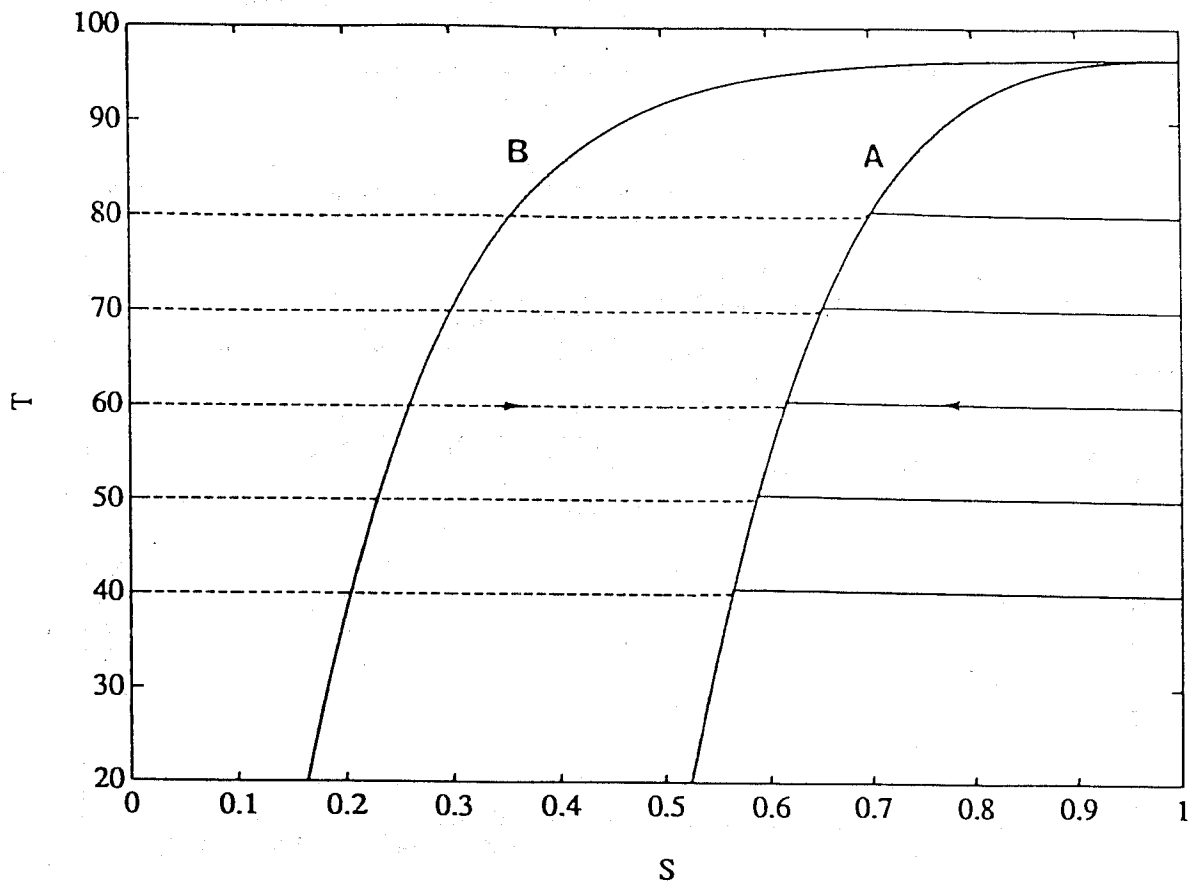


Figure 8: Phase Portrait and (T, S) Trajectories for Propane at Conditions of Miller (1951). Arrow Indicates Upstream Direction.

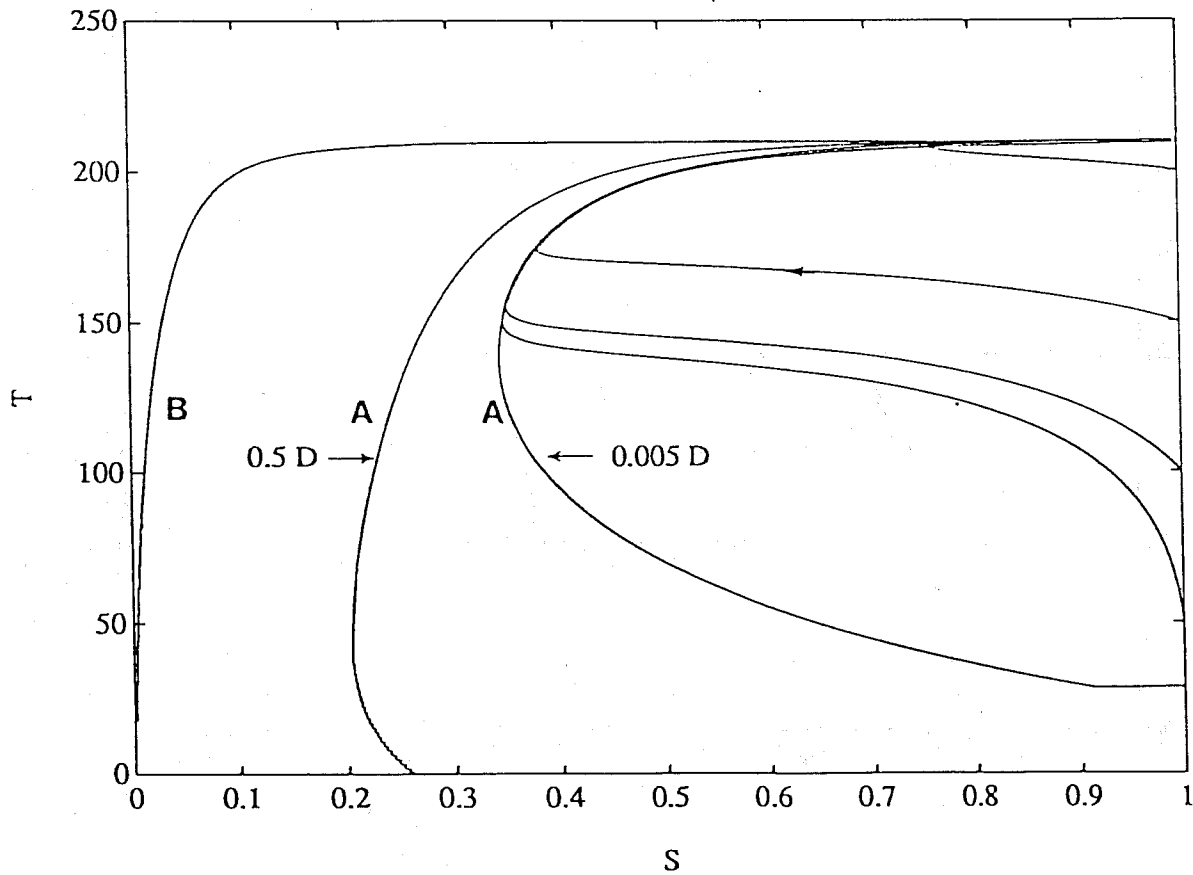


Figure 9: Phase Portrait and (T, S) Trajectories for Water at Conditions of Table 2. Effect of Permeability. Arrow Indicates Upstream Direction.

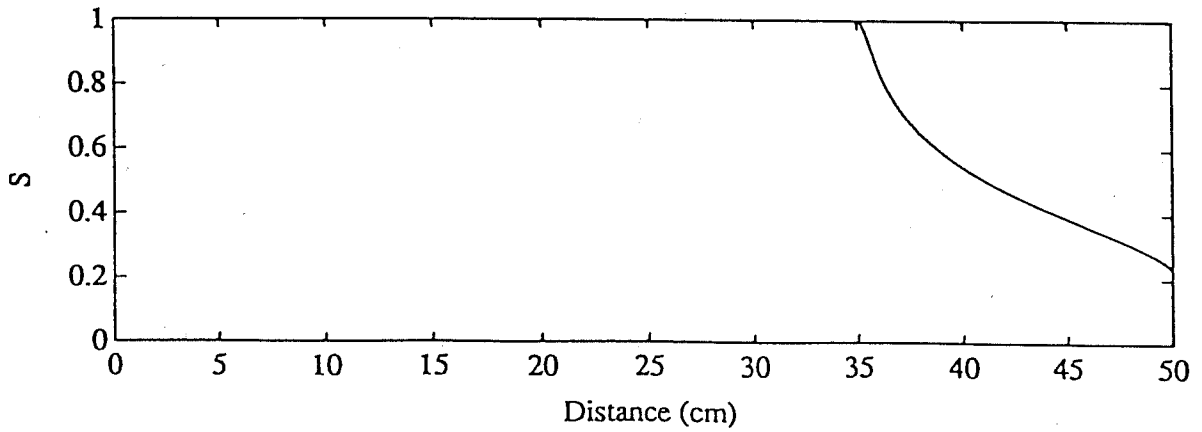
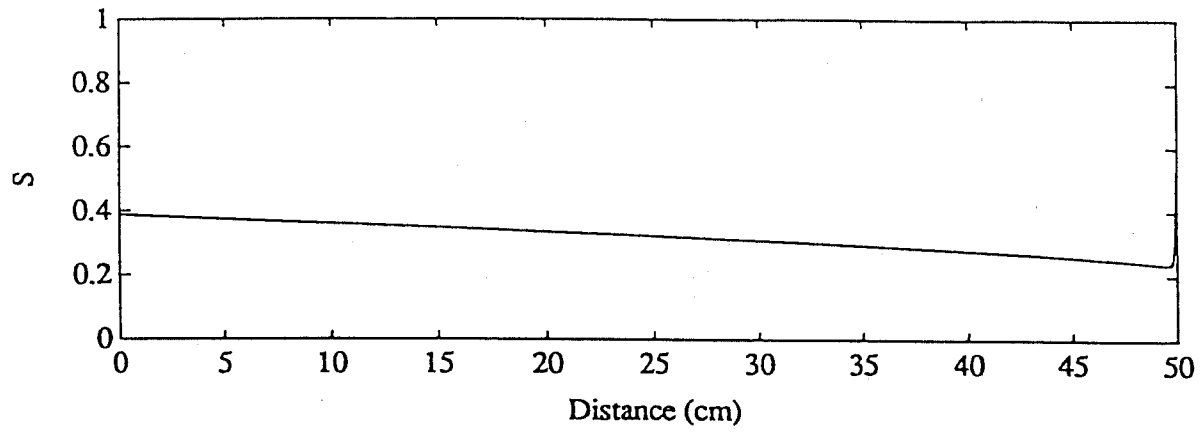
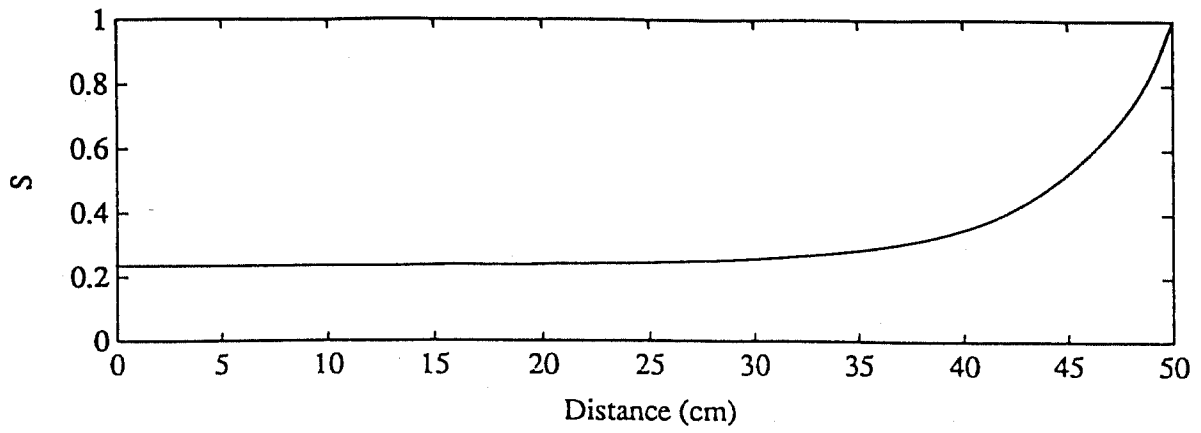


Figure 10: Sensitivity of Saturation Profiles to the Rate Parameter R_m ($R_m = 0.01, 1, 10$ from top to bottom).

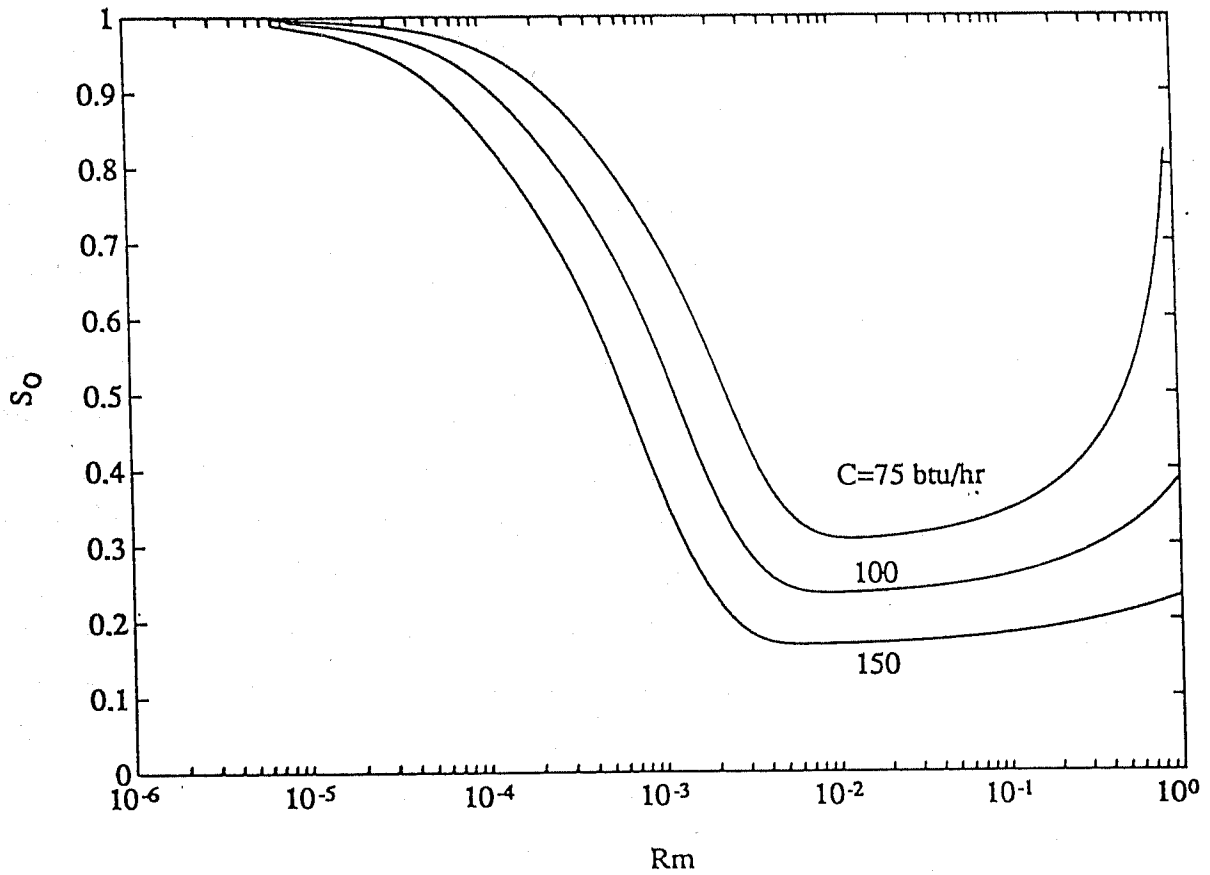


Figure 11: Sensitivity of Inlet Saturation (S_0) to the Rate Parameter R_m for Standard Conditions: Effect of Heat Injection Rate C (btu/hr).

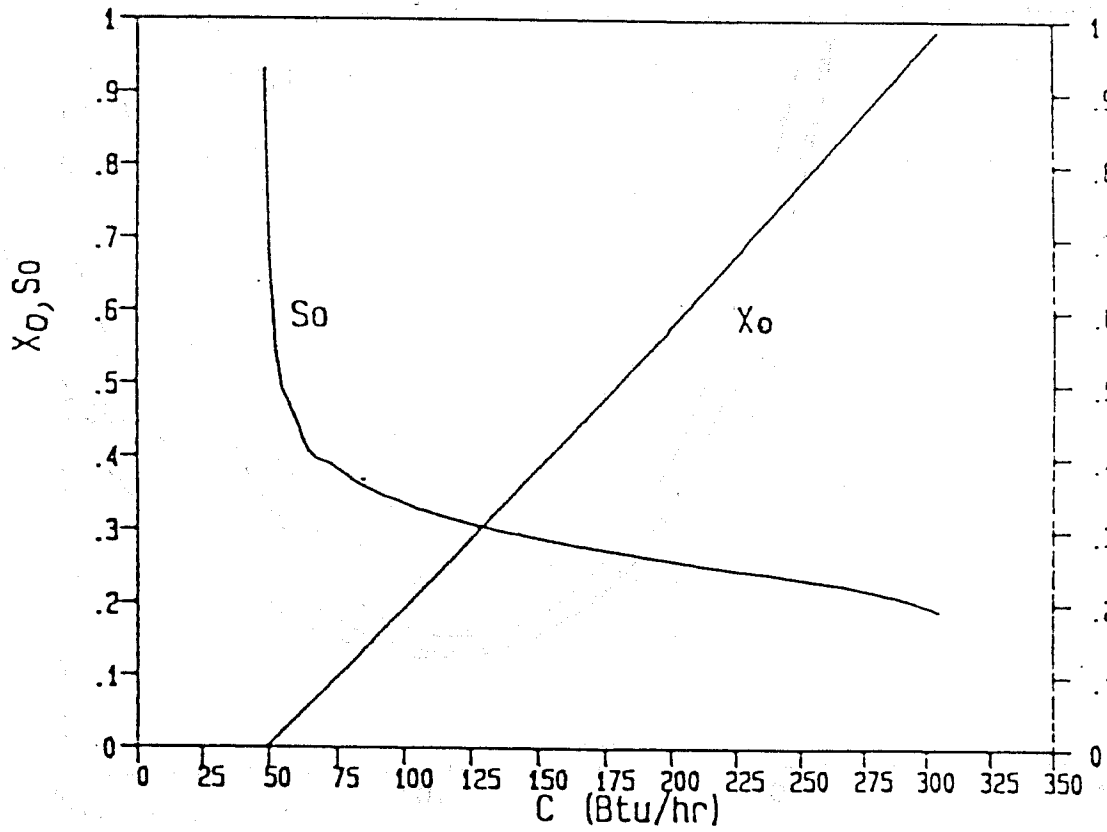


Figure 12: Sensitivity of Inlet Saturation to Steam Quality and Heat Injection Rate for the Conditions of Sanchez and Schechter (1987).

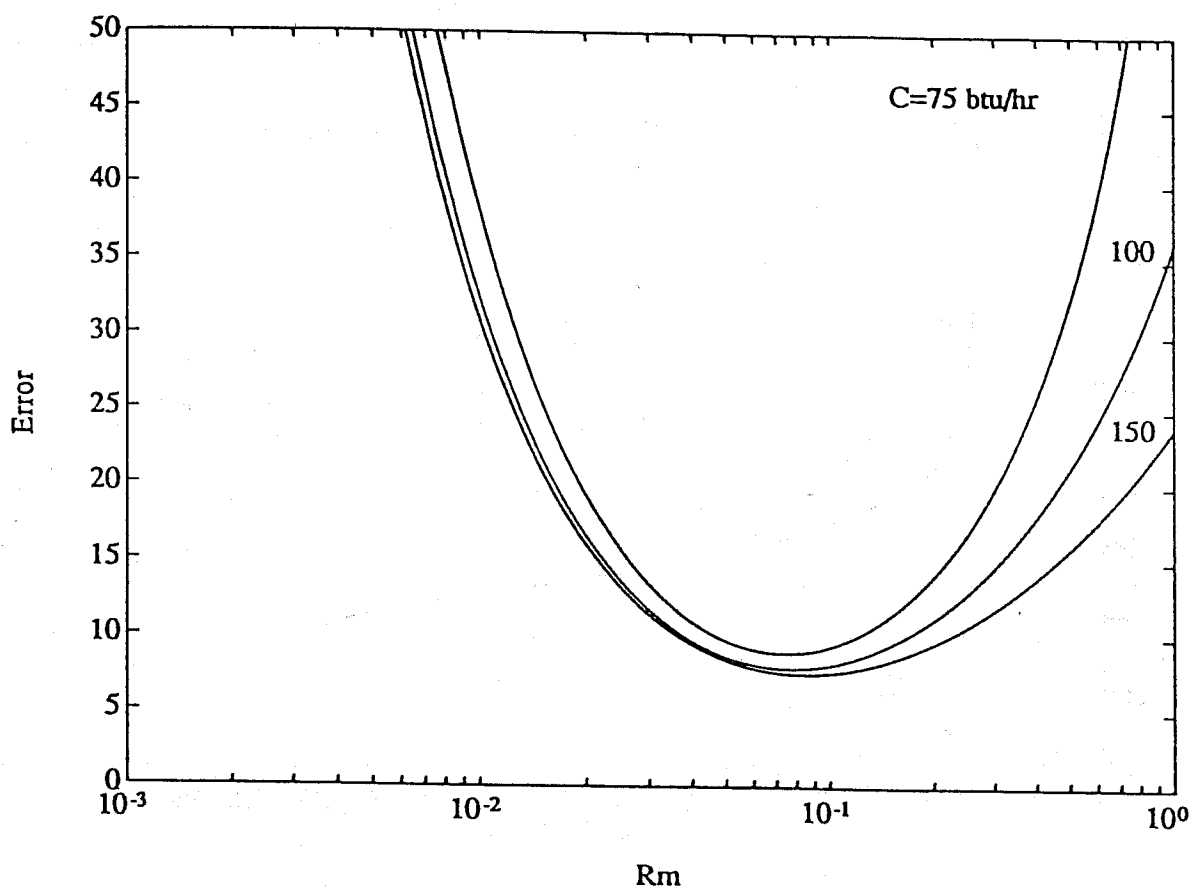


Figure 13: Sensitivity of Error Estimate to the Rate Parameter R_m for Standard Conditions: Effect of Heat Injection Rate C (btu/hr).

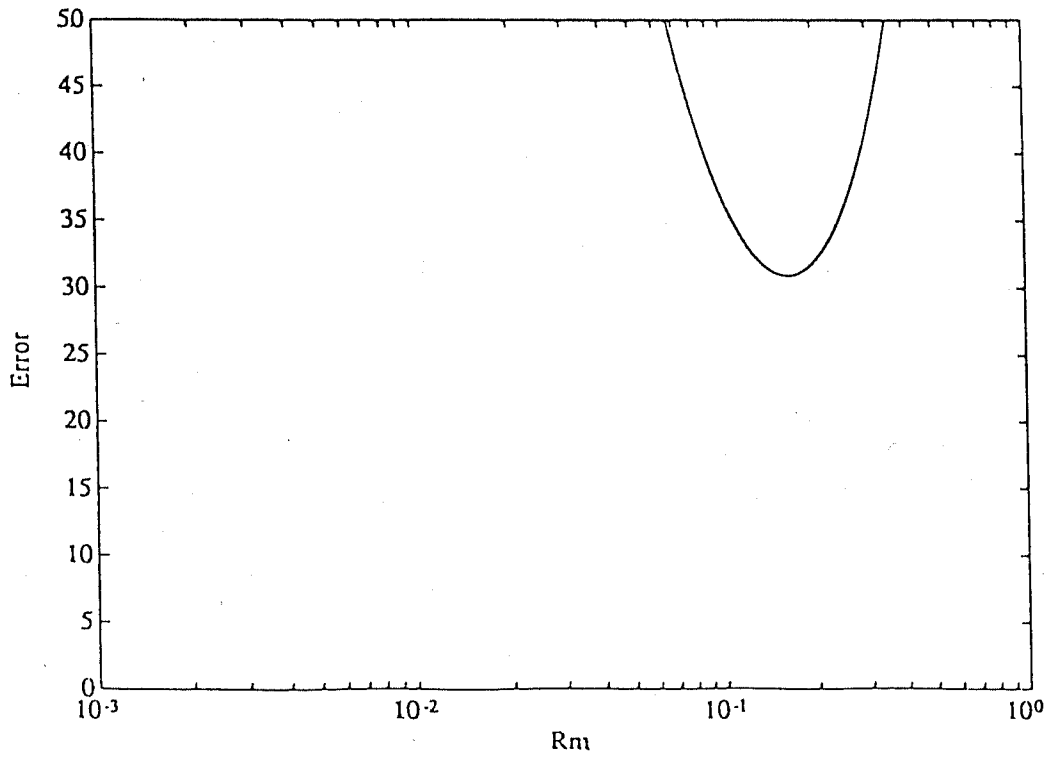
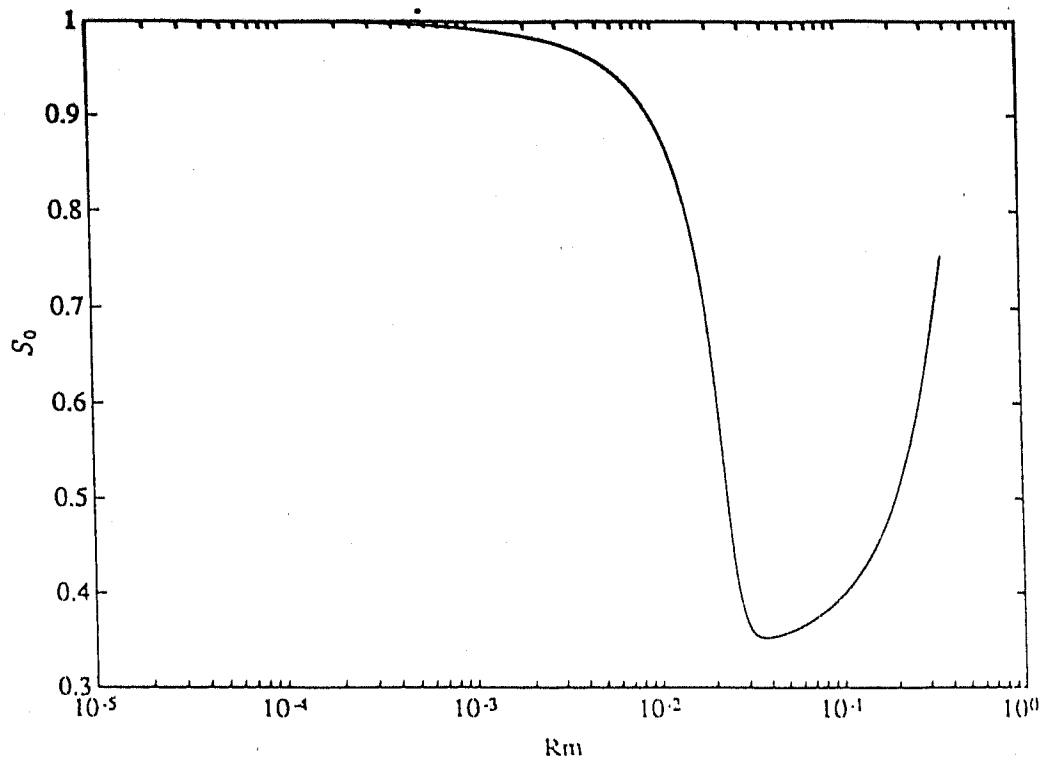


Figure 14: Sensitivity of Inlet Saturation and Error Estimate to the Rate Parameter R_m for Standard Conditions and Permeability of $0.005d$.

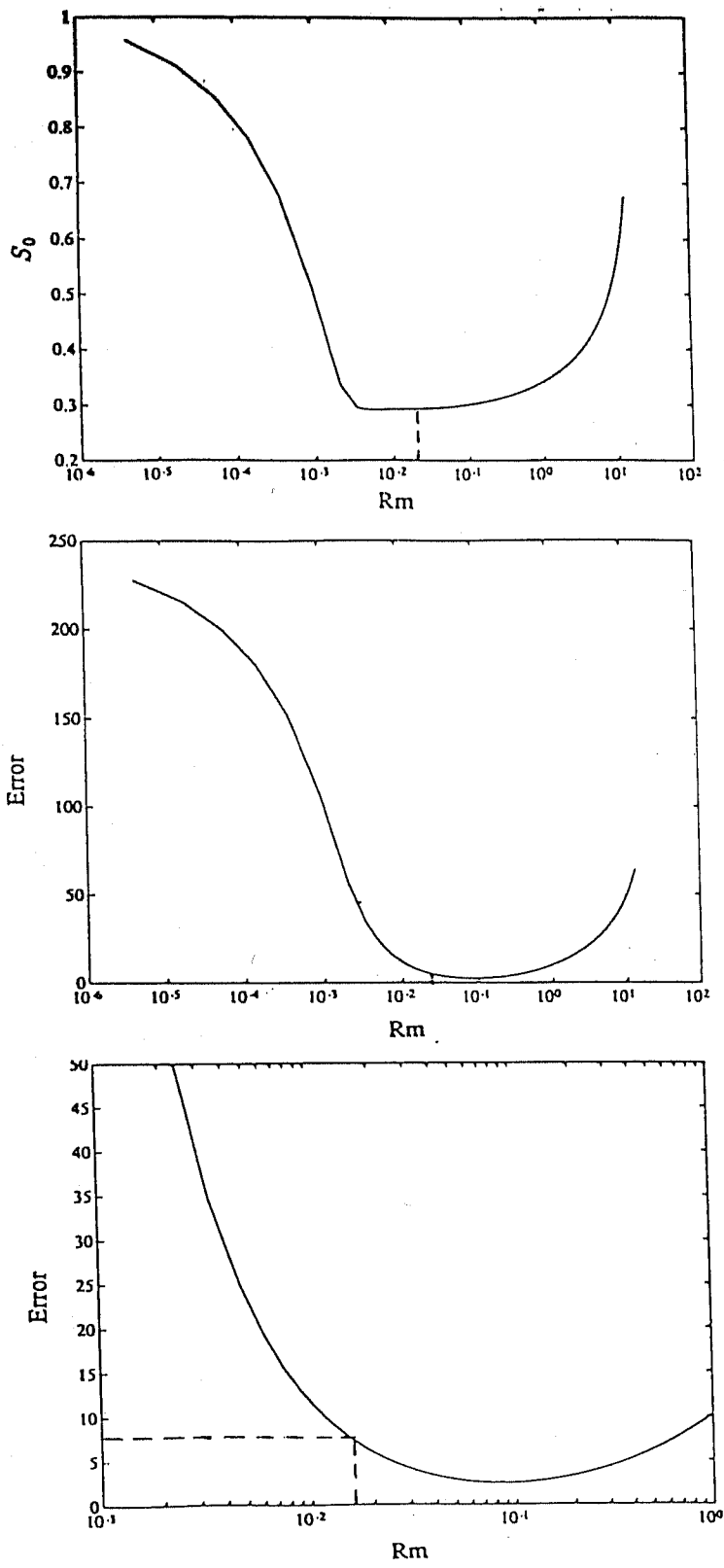


Figure 15: Sensitivity of Inlet Saturation and Error Estimate (at two different magnifications) to the Rate Parameter R_m for Conditions of Run 15 in Sanchez and Schechter (1987).



